

Musical Instrument Separation on Shift-Invariant Spectrograms via Stochastic Dictionary Learning

Sören Schulze, Emily J. King

Abstract—We propose a novel method for the blind separation of audio signals produced by musical instruments. While the approach of applying non-negative matrix factorization (NMF) has been studied in many papers, it does not make use of the pitch-invariance that the sounds of instruments exhibit. This limitation can be overcome by using tensor factorization, in which context the use of log-frequency spectrograms was initiated, but this still requires the specific tuning of the instruments to be hard-coded into the algorithm. We develop a time-frequency representation that is both shift-invariant and frequency-aligned, with a variant that can also be used for wideband signals. Our separation algorithm exploits this shift-invariance in order to find patterns of peaks related to specific instruments, while non-linear optimization enables it to represent arbitrary frequencies and incorporate inharmonicity, and the reasonability of the representation is ensured by a sparsity condition. The relative amplitudes of the harmonics are saved in a dictionary, which is trained via a modified version of ADAM. For a realistic monaural piece with acoustic recorder and violin, we achieve qualitatively good separation with a signal-to-distortion ratio (SDR) of 12.5 dB, a signal-to-interference ratio (SIR) of 25.7 dB, and a signal-to-artifacts ratio (SAR) of 12.7 dB, averaged.

Index Terms—Blind source separation, unsupervised learning, acoustic signal processing, spectrogram, music information retrieval, dictionary learning, sparsity, stochastic optimization, constant-Q transform, ADAM, orthogonal matching pursuit

I. INTRODUCTION

A. Problem Definition, Related Work, and Approach

THE *source separation* problem concerns itself with the recovery of signals X_1, \dots, X_c from a mixture $X = X_1 + \dots + X_c$. We speak of *blind separation* when no specific prior information to characterize the sources of the signals is provided.

Dictionary learning is the process of computing a collection of *atoms* whose linear combination is used to approximate the target data. This technique is very popular for the blind separation of audio sources, both of music recordings as well as of speech signals.

In order to apply dictionary learning on audio data, it is helpful to regard a time-frequency representation which subdivides the problem into smaller time frames and highlights the frequency characteristics of the signal. Classically, such a representation is computed via application of the short-time Fourier transform (STFT) (cf. [1]) on the audio signal, and the resulting spectrogram (i.e., the magnitude of the STFT) is then decomposed via non-negative matrix factorization (NMF) [2] in order to obtain a dictionary. This approach was initially studied

by Smaragdis and Brown [3] for the purpose of polyphonic music transcription and then applied to audio source separation by Wang and Plumbley [4].

In many cases, a single musical instrument can generate different sounds which are perceptually similar but only vary in the pitch of the tones. In the STFT spectrogram, different pitch manifests in linear scaling of the distances between the peaks in the frequency axis, which is computationally hard to handle. Therefore, Fitzgerald et al. [5] applied the constant-Q transform (CQT) [6], which turns scaling into shifts, and developed the shifted non-negative matrix factorization (SNMF), that is actually a tensor factorization, in order to train a shift-invariant dictionary. This approach was later refined by Jaiswal et al. [7], [8], [9].

While the constant-Q transform ensures the shift-invariance of patterns of sinusoids when varying the pitch, its transient response varies with frequency. To overcome this, the scattering transform by Andén and Mallat [10] subsequently employs smoothing in the time domain.

Another approach is the computation of the Mel spectrogram [11], which applies logarithmically spaced windows in the frequency direction. This, however, unfavorably amplifies transients in the higher frequencies.

The Heisenberg uncertainty principle (cf. [1], [12]) sets a fundamental bound to the time-frequency resolution achievable. If we use Gaussian windows where ζ is the standard deviation of the window in the time domain and σ is the standard deviation of its Fourier transform, then we have $\zeta \cdot \sigma = 1/(2\pi)$. If, for instance, $\zeta = 20$ ms, then $\sigma \approx 7.96$ Hz. For speech processing, this may be sufficient, but considering music that contains frequencies as low as 20 Hz, this deviation equals almost half an octave (or a tritone).

Whereas this low resolution may be acceptable for low frequencies where tight intervals are rare, conveying it to higher frequencies for the sake of shift-invariance is infeasible. Instead, we rely on sparsity-based techniques and prior information about the images of the tones in the spectrogram in order to sharpen the lines beyond the limit determined by the Heisenberg uncertainty principle.

B. The Musical Role of Sparsity

The representation of the time frames of a spectrogram of a music recording with a dictionary is in general not unique. If we consider wind and string instruments, their sound is dominated by a linear combination of sinusoids, which show up as horizontal lines in the spectrogram. Thus, there exists a trivial solution that assumes a single sinusoidal instrument

The authors are with the working group Computational Data Analysis, Faculty 3, University of Bremen, Bibliothekstr. 5, 28359 Bremen, Germany (e-mail: sschulze@math.uni-bremen.de, king@math.uni-bremen.de).

which plays a large number of simultaneous tones. While this solution is valid, it is undesirable, as no separation is performed at all.

A similarly trivial solution is to construct different instruments for each time frame of the spectrogram. In this case, matching the constructed instruments with the actual instruments requires a lot of manual post-processing; also, instruments which play harmonically related notes may be mistaken for a single instrument, so this representation is again problematic for separation.

In order to attain meaningful solutions, it is essential to limit both the total number of instruments and the number of tones that are assumed to be played at the same time. The former is controlled by the layout of the dictionary, while the latter is a sparsity condition that requires the use of appropriate algorithms.

The constraints imposed by these numbers are supposed to encourage solutions that will appear meaningful to a human listener. Good results can be achieved if both numbers are known and sufficiently low, but blind separation meets its conceptual limits in case of very polyphonic works such as orchestral symphonies. One particularly difficult instrument is the pipe organ, where the combination of organs stops blurs the borders of what should be considered a single instrument (cf. [13], [14]).

C. Structure of this Paper

In Section II, we propose two novel time-frequency representations (spectrograms) with a logarithmic frequency axis. One of them is a modification to the scattering transform, and it is designed to be shift-invariant and frequency-uniform at the same time. While this representation is good for narrowband signals, it suffers from loss of accuracy when applied to wideband signals due to the Heisenberg uncertainty principle. Thus, we define another method which overcomes this limitation via the application of sparse pursuit on the linear-frequency spectrogram.

In Section III, we define our dictionary representation for time frames of the spectrogram. It is perfectly pitch-invariant, which means that any real number in the regarded frequency range can be assumed as the fundamental frequency of a tone. For optimization, we propose a modified least-squares loss, which equalizes the amplitudes of the peaks in order to attach higher importance to higher harmonics.

In Section IV, we expound our algorithmic approach: Our novel algorithm is a modified version of orthogonal matching pursuit (OMP) with a non-linear optimization step for refinement, which makes it capable of representing arbitrary tones at arbitrary tuning, with individually identified inharmonicity. For dictionary learning, we employ a modified version of ADAM, which is a popular stochastic gradient descent algorithm that was initially developed for the training of deep neural networks. Our modifications adapt this algorithm to dictionary learning, preserving the relative scaling of certain components of the gradient and periodically resetting parts of the dictionary as needed.

In Section V, we evaluate the performance of the overall algorithm via standard measures; we identify its strengths and

weaknesses, and we compare it to algorithms proposed in other works that follow a similar approach. We further present parts of the computational result on realistic audio data via spectrograms and give a qualitative assessment of the results.

II. COMPUTATION OF THE SPECTROGRAM

A. Narrowband Signals

The dictionary learning algorithm that we develop is supposed to operate on a spectrogram, which is a non-negative time-frequency representation of the audio recording. We require the spectrogram to be shift-invariant, such that multiplying the frequency of a sinusoidal signal by a fixed factor induces a fixed shift of its image in the spectrogram. At the same time, the image of a δ -transient should be uniform along the frequency axis.

The first requirement is fulfilled by the CQT introduced by Brown [6]; this method was later generalized by Balazs et al. [15]. In the scattering transform [10], the CQT is interpreted as a Morlet wavelet transform; afterwards, the modulus is convolved with a smoothing kernel in order to widen the transient response in the higher frequencies.

We take this concept a step further by designing the kernel such that the transient response is frequency-uniform. First of all, we consider the continuous constant-Q transform $Y: \mathbb{R} \times \mathbb{R} \rightarrow \mathbb{C}$ of a signal $X \in L_\infty(\mathbb{R})$ with a window $w \in L_1(\mathbb{R})$, both of which are real-valued:

$$\begin{aligned} Y(f, t) &= Q_w X(f, t) \\ &:= \frac{|f|}{f_{\min}} \int_{-\infty}^{\infty} X(s) w\left(\frac{f}{f_{\min}}(s-t)\right) e^{-i2\pi fs} ds, \end{aligned}$$

where $f_{\min} > 0$ is a scaling factor.

The resulting spectrogram is shift-invariant: If we consider $X(t) = \cos(2\pi\nu t)$ with $\nu > 0$, then the resulting constant-Q transform is:

$$\begin{aligned} Y(f, t) &= \frac{|f|}{f_{\min}} \int_{-\infty}^{\infty} \frac{e^{-i2\pi\nu s} + e^{i2\pi\nu s}}{2} w\left(\frac{f}{f_{\min}}(s-t)\right) e^{-i2\pi fs} ds \\ &= \frac{1}{2} \mathcal{F}w\left(f_{\min}\left(1 + \frac{\nu}{f}\right)\right) e^{-i2\pi(f+\nu)t} \\ &\quad + \frac{1}{2} \mathcal{F}w\left(f_{\min}\left(1 - \frac{\nu}{f}\right)\right) e^{-i2\pi(f-\nu)t}, \end{aligned}$$

where $\mathcal{F}: L_1(\mathbb{R}) \rightarrow L_\infty(\mathbb{R})$ is the Fourier transform operator (cf. [16], [17], [1]) with:

$$\mathcal{F}w(f) := \int_{-\infty}^{\infty} w(t) e^{-i2\pi ft} dt.$$

For $f > 0$, the first summand is zero if $\text{supp}(\mathcal{F}w) \subseteq [-f_{\min}, f_{\min}]$. The modulus of the second summand only depends on the ratio ν/f , making the magnitude of the spectrogram shift-invariant on a logarithmic frequency axis.

We would like to select w and therefore also $\mathcal{F}w$ as Gaussians with standard deviations ζ and $\sigma = 1/(2\pi\zeta)$, but then they will have unbounded support. This means that we must choose f_{\min} large enough such that $\mathcal{F}w$ has

sufficiently decayed at this frequency. We obtain the logarithmic frequency via the transform $\alpha(f) = \alpha_0 \ln(f/f_0)$ with arbitrary parameters $\alpha_0, f_0 > 0$; inversely, the linear frequency is recovered via $f(\alpha) = f_0 e^{\alpha/\alpha_0}$. For the magnitude of the dominant term in $Y(f, t)$, we then have:

$$\begin{aligned} & \mathcal{F}w\left(f_{\min}\left(1 - \frac{\nu}{f}\right)\right) \\ &= \mathcal{F}w\left(f_{\min}\left(1 - \frac{\nu}{f_0 e^{\alpha/\alpha_0}}\right)\right) \\ &= \sqrt{2\pi}\zeta f_{\min} \exp\left(\frac{(2\pi\zeta f_{\min})^2}{2}\left(1 - \frac{\nu}{f_0 e^{\alpha/\alpha_0}}\right)^2\right), \end{aligned}$$

which is not Gauss-shaped when regarded as a function of α , but we can approximate the mapping $\alpha \mapsto 1 - \frac{\nu}{f_0 e^{\alpha/\alpha_0}}$ by its linear approximation at $\alpha = \alpha_0 \ln(\nu/f_0)$:

$$1 - \frac{\nu}{f_0 e^{\alpha/\alpha_0}} = \frac{\alpha - \alpha_0 \ln(\nu/f_0)}{\alpha_0} + O((\alpha - \alpha_0 \ln(\nu/f_0))^2),$$

leading to a scaled Gaussian with mean $\mu = \alpha_0 \ln(\nu/f_0)$ and standard deviation $\sigma = \alpha_0/(2\pi\zeta f_{\min})$. Again, the validity of this approximation depends on the value of $\mathcal{F}w(f_{\min})$.

To check the second requirement, we need to regard the generalized Fourier transform on the space of tempered distributions:

$$Y(f, t) = \mathcal{Q}_w X(f, t) := \mathcal{F}\Xi_{f,t}(f),$$

where

$$\Xi_{f,t} = \frac{|f|}{f_{\min}} X \cdot w\left(\frac{f}{f_{\min}}(\cdot - t)\right),$$

with $X \in \mathcal{S}'(\mathbb{R})$, $w \in \mathcal{S}(\mathbb{R})$, and with $\mathcal{F}\Xi_{f,t} \in \mathcal{S}'(\mathbb{R})$ assumed to be representable as a complex-valued function (cf. [16] for the mathematical background).

For the reponse to a δ -transient at $t = t_0$, we then obtain:

$$Y(f, t) = \frac{|f|}{f_{\min}} w\left(\frac{f}{f_{\min}}(t_0 - t)\right) e^{-i2\pi f t_0},$$

whose modulus is not frequency-uniform. On the other hand, we know that if w is Gauss-shaped, we can convolve it with another Gaussian in order to attain the same variance for all frequencies. We thus define:

$$\begin{aligned} U(\alpha, t) &:= \frac{f(\alpha)}{\sqrt{f(\alpha)^2 - f_{\min}^2}} \cdot \\ &\int_{-\infty}^{\infty} |\mathcal{Q}_w X(f(\alpha), t - s)| w\left(\frac{f(\alpha)}{\sqrt{f(\alpha)^2 - f_{\min}^2}} s\right) ds, \end{aligned}$$

with $w(s) = e^{-s^2/(2\zeta^2)}/\sqrt{2\pi\zeta^2}$. This is only valid for $f(\alpha) > f_{\min}$. For $f(\alpha) = f_{\min}$, we can just use $|\mathcal{Q}_w X(f_{\min}, t)|$ without the convolution, but for $f(\alpha) < f_{\min}$, we would need to solve a deconvolution problem, which is ill-posed. This means that f_{\min} is actually the minimum frequency which can be resolved in the spectrogram.

It is natural to choose $f_0 = f_{\min}$. In this case, $\alpha(f_{\min}) = \alpha(f_0) = 0$, while α_0 can still be used to scale the frequency axis.

In practice, the convolution is carried out in the discrete domain, which introduces some error, but with sufficiently

large resolution, this is rather low. It is, however, important to fix the ℓ_1 norm of the convolution kernel.

Recently, a similar time-frequency representation was developed by Dörfler et al. [18]: It was shown that when smoothing the *squared* magnitude of the CQT along the time axis, the result is equivalent to a Mel spectrogram. However, as squaring alters the ℓ_1 norm, the resulting transient response will no longer be frequency-uniform; instead, the magnitude grows linearly with frequency, so while the shift-invariance of the sinusoids is kept intact, transients will be amplified in the higher frequencies. Thus, while this representation is easier to compute, it does not have the properties that we desire.

B. Wideband Signals

The problem with the previously discussed computation of the spectrogram comes from the Heisenberg uncertainty principle: Frequencies below f_{\min} cannot be resolved because the time-domain response would be too long, and setting f_{\min} too low deteriorates the frequency resolution and introduces artifacts.

In general, any attempt to overcome this limitation would lead to an ill-posed problem. On the other hand, we know that the sound of many musical instruments can be represented as a sum of sinusoids, which correspond to Gaussian peaks in the frequency domain. With the short-time Fourier transform (cf. [1])

$$Z(f, t) = \mathcal{F}_w X(f, t) := \int_{-\infty}^{\infty} X(s) w(s - t) e^{-i2\pi f s} ds$$

and $X(t) = \cos(2\pi\nu t)$, we get:

$$Z(f, t) = \frac{1}{2} \mathcal{F}w(f + \nu) e^{-i2\pi(f + \nu)t} + \frac{1}{2} \mathcal{F}w(f - \nu) e^{-i2\pi(f - \nu)t}.$$

In Section IV-A, we introduce Algorithm 2 that can be used to identify patterns of peaks in a given logarithmic frequency spectrum. We can use the same algorithm to identify individual peaks in the linear frequency spectrum $Z(\cdot, t)$ (or rather its discretized version $Z[\cdot, k]$), apply the logarithm to their position, and thereby mimic the effect of the constant-Q transform while also preserving vertical alignment.¹ This “tricks” the Heisenberg uncertainty principle by using prior information about the shape of the peaks.

With this method, we can choose f_0 to be the lowest frequency that we aim to represent, while f_{\min} is merely a virtual quantity that indicates the frequency at which the same time-frequency resolution could still be achieved by the narrowband method.

III. INSTRUMENT DICTIONARY REPRESENTATION OF THE SIGNAL

A. Dictionary Layout and Parameters

Our dictionary is a two-dimensional data structure $D \in \mathbb{R}^{N_{\text{har}} \times N_{\text{ins}}}$, which is used to represent a discrete magnitude

¹For efficiency, we choose parameters $p = q = 1$. We assume a single instrument with $N_{\text{har}} = 1$ and set a sparsity condition of $N_{\text{ton}} = 1000$ with $\lambda = 1$ and $N_{\text{itr}} = 20$. Rather than selecting one frequency with the highest cross-correlation at a time, we select the 1000 highest peaks with a dominance of more than 2 pixels.

spectrogram $U[\alpha, k]$, $\alpha, k \in \mathbb{Z}$, with $U[\alpha, k] = U(\alpha, t)$, $k = t/\gamma$, where $\gamma > 0$ is the time-sampling period for the spectrogram (with the scaling of the frequency axis determined by α_0). The number of tones is limited to N_{ton} . For each $k = 1, \dots, n$, we declare an index set $\mathcal{J}_k \subset \mathbb{N}$ for the parameters $a_{k,j}, \mu_{k,j}, \sigma_{k,j}, b_{k,j} \geq 0$ and $\eta_{k,j} \in \{1, \dots, N_{\text{ins}}\}$, $j \in \mathcal{J}_k$, where $a_{k,j}$ is the amplitude of a certain instrument tone, $\mu_{k,j}$ is the logarithmic fundamental frequency, $\sigma_{k,j}$ is the standard deviation of the corresponding Gaussian, $b_{k,j}$ is the inharmonicity, and $\eta_{k,j}$ is the selected instrument.

A simple model for many musical instruments is the wave equation, which has sinusoidal solutions at frequencies $f_h = hf_1^\circ$, $h = 1, \dots, N_{\text{har}}$, where $f_1^\circ > 0$ is the fundamental frequency. However, many string instruments (especially the piano with its high-tension strings) have non-negligible stiffness in their strings, leading to a fourth-order equation, which has solutions $f_h = (1 + bh^2)^{1/2}hf_1^\circ$, with the inharmonicity parameter $b > 0$ (cf. [13]). Applying the logarithm to both sides, this leads to $\ln(f_h) = \frac{1}{2}\ln(1 + bh^2) + \ln(hf_1^\circ)$.

Thus, a simple model for generating the spectrogram is:

$$u[\alpha, k] = \sum_{j \in \mathcal{J}_k} \sum_{h=1}^{N_{\text{har}}} a_{k,j} D[h, \eta_{k,j}] \cdot \exp\left(-\frac{(\alpha - \mu_{k,j} - \alpha_0 (\ln(h) + \frac{1}{2}\ln(1 + b_{k,j}h^2)))^2}{2\sigma_{k,j}^2}\right),$$

with $\alpha, k \in \mathbb{Z}$, and with $\alpha_0 > 0$ from Section II-A. However, the magnitude spectrogram is not linear; in general, tones will interfere, creating beats. If the signals are uncorrelated (i.e., their inner product is 0), the squares will add linearly; to account for this, we define:

$$(u_p[\alpha, k])^p := \sum_{j \in \mathcal{J}_k} a_{k,j}^p (u_{p, \eta_{k,j}}[\alpha, k])^p$$

with

$$(u_{p, \eta, j}[\alpha, k])^p := \sum_{h=1}^{N_{\text{har}}} D[h, \eta]^p \cdot \exp\left(-\frac{(\alpha - \mu_{k,j} - \alpha_0 (\ln(h) + \frac{1}{2}\ln(1 + b_{k,j}h^2)))^2}{2\sigma_{k,j}^2}\right)^p,$$

choosing $p = 2$.

B. Loss Term and Non-Linear Scaling

From one of the methods of either Section II-A or Section II-B, we are given a measured magnitude spectrogram $U = (U[\alpha, k])_{\alpha, k \in \mathbb{Z}}$, which in practice has a finite size, such that $\text{supp}(U) \subseteq \{0, \dots, m-1\} \times \{0, \dots, n-1\}$, with $m, n \in \mathbb{N}$.

The straight-forward loss term is then given by the Frobenius norm as $R_{\mathcal{K}} = \frac{1}{2} \|U[\cdot, \mathcal{K}] - u_2[\cdot, \mathcal{K}]\|_{\mathbb{F}}$, where \mathcal{K} is either an index set or a single index. However, it turns out that this is not a good distance measure for clustering tones from different instruments; this loss puts a large penalty on deviations in the lowest harmonics, but it is hardly influenced by the presence of higher harmonics.

The problem is that higher harmonics typically decay very quickly in power and are thus ignored by the Frobenius norm, while the human ear can still perceive them clearly. Our heuristic approach is to ‘‘lift’’ those harmonics using a concave power function:

$$R_{\mathcal{K}, q} := \frac{1}{2} \left\| (U[\cdot, \mathcal{K}])^q - (u_2[\cdot, \mathcal{K}])^q \right\|_{\mathbb{F}}^2, \quad 0 < q \leq 1.$$

The right choice of q is always a compromise: Choosing it too close to 1 will not have a sufficient effect, but choosing it too low makes the problem very non-convex, leading to computational issues. In practice, square root scaling with $q = 1/2$ produces good results.

IV. ALGORITHMIC APPROACH

In order to train the dictionary, we pursue a stochastic alternating-optimization approach. First the dictionary is initialized; for each $\eta = 1, \dots, N_{\text{ins}}$, we generate a uniformly distributed random vector $d \in [0, 1]^{N_{\text{har}}}$ and an exponent $e \in [1, \infty)$ that is Pareto-distributed with a scale parameter of 2, and we set $D[h, \eta] = d[h]/h^e$. The initialization function and the main procedure are listed in Algorithm 1.

```

function init()
  e ← Par(1, 2)
  for h = 1, ..., Nhar do
    d[h] ← U[0, 1]
    d[h] ← d[h]/he
  return d[·]
for η = 1, ..., Nins do
  D[·, η] ← init()
  τ[η] ← 0, v1[·, η] ← 0, v2[η] ← 0, A[η] ← 0
loop a multiple of Nprn times
  k ← random({0, ..., n-1})
  Jk, ak, Jk, μk, Jk, σk, Jk, bk, Jk, ηk, Jk, A
  ← pursuit(D, U, k, A)
  D, τ, v1, v2 ← adam(D, τ, v1, v2, U, k, Jk,
    ak, Jk, μk, Jk, σk, Jk, bk, Jk, ηk, Jk)
  if min(τ) mod Nprn = 0 then
    J, τ, v1, v2, A ← renew(A)
for k = 0, ..., n-1 do
  Jk, ak, Jk, μk, Jk, σk, Jk, bk, Jk, ηk, Jk, A
  ← pursuit(D[·, J], U, k, A)

```

Figure 1. Dictionary initialization and main program

Given an initial dictionary, a random time frame $U[\cdot, k]$ of the measured spectrogram is chosen, and a sparse dictionary representation is computed. Afterwards, the dictionary is updated and the process is repeated.

A. Sparse Identification

The pursuit algorithm (Algorithm 2) is roughly based on orthogonal matching pursuit (OMP) [19], but it also incorporates ideas from subspace pursuit [20]. For each $k = 0, \dots, n-1$,

the parameters are initialized as $a_{k,j}, b_{k,j}, \mu_{k,j} = 0$ and $\sigma_{k,j} = \alpha_0 / (2\pi\zeta f_{\min})$ for $j = 1, \dots, N_{\text{ton}} + 1$. The residual is initialized with $r_k = (U[\cdot, k])^q$.

In each step, an index $j \in \{1, \dots, N_{\text{ton}} + 1\}$ with $a_{k,j} = 0$ is picked. The cross-correlation between the residual and the spectra of the individual instruments is computed as:

$$\rho_{k,j}[\alpha, \eta] = \sum_{i=0}^{m-1} \frac{r_k[i] (u_{2,\eta,j}[i - \alpha, k])^q}{\|(u_{2,\eta,j}[\cdot, k])^q\|_2}.$$

In order to accelerate this computation via the FFT (cf. [21]), it is favorable to choose m as a power of 2.

Then, $\alpha \in \{0, \dots, m - 1\}$ and $\eta \in \{1, \dots, N_{\text{ins}}\}$ are chosen such that $\rho_{k,j}[\alpha, \eta]$ is maximized, and they are assigned to $\mu_{k,j}$ and $\eta_{k,j}$. The amplitude is set to $a_{k,j}^q \leftarrow \rho_{k,j}[\mu_{k,j}, \eta_{k,j}] / \|(u_{2,\eta_{k,j},j}[\cdot, k])^q\|_2$.

After this, for all the indices $j = 1, \dots, N_{\text{ton}} + 1$ for which $a_{k,j} > 0$ holds, the values $a_{k,j}, \mu_{k,j}, \sigma_{k,j}, b_{k,j}$ are refined via non-linear optimization in order to minimize R_q . For this purpose, we use the L-BFGS-B algorithm [22], [23], [24]. Then, all tones but the ones with the N_{ton} highest positive amplitudes are excluded and reinitialized, and the non-linear optimization process is run again.

In preparation for the next step, the residual is updated as $r_k \leftarrow (U[\cdot, k])^q - (u_2[\cdot, k])^q$. The parameters for the tones with positive amplitudes are retained, and the others are reinitialized.

It is required that each step decreases the Euclidean norm of the residual by factor of at least $1 - \lambda$, with $\lambda \in (0, 1]$; otherwise, the result of the current step is discarded, and the parameters from the previous step are returned. The total number of iterations is limited to a value that is appropriate for the number of tones to identify; we choose $N_{\text{itr}} = 2N_{\text{ton}}$.

B. Dictionary Update

Classically, dictionary learning is performed via techniques like NMF [2], [25], K-SVD [26], or tensor factorization. However, the first two methods do not account for our shift-invariant structure of the data. The latter does, but only for a fixed number of frequency shifts. Moreover, all of these methods become slow when the amount of data is large.

While the use of stochastic gradient descent for dictionary learning has been common for many years (cf., e.g., [27]), new methods have been arising very recently due to their applications in deep learning. One of the most popular methods for this purpose is ADAM [28]. Its underlying idea is to treat the gradient as a random variable and, for each component, estimate its first moments as v_1 and its second moments as v_2 , and choose the step size proportional to $v_1/\sqrt{v_2}$. If the derivative of the i th component is constant, then $v_1[i]/\sqrt{v_2[i]} = \pm 1$, in which case a large step size can be used. If the derivative oscillates a lot, however, then $v_1[i]/\sqrt{v_2[i]}$ will also be small and thereby dampen the oscillation in that direction.

The standard formulation of ADAM is completely independent of the scale of the derivatives. This makes it easy to control the absolute step size of the components, but it destroys the Landweber regularization property of gradient descent, which automatically decreases the step size for components whose

function pursuit(D, U, k, A)

```

 $r_k \leftarrow (U[\cdot, k])^q$ 
 $\mathcal{J}_k \leftarrow \emptyset$ 
loop  $N_{\text{itr}}$  times
   $a_{k,j}, b_{k,j}, \mu_{k,j} \leftarrow 0, \sigma_{k,j} \leftarrow \alpha_0 / (2\pi\zeta f_{\min})$ 
  for  $j \in \{1, \dots, N_{\text{ton}} + 1\} \setminus \mathcal{J}_k$ 
     $j \leftarrow \min(\{1, \dots, N_{\text{ton}} + 1\} \setminus \mathcal{J}_k)$ 
     $\rho_{k,j}[\alpha, \eta] \leftarrow \sum_{i=0}^{m-1} r_k[i] (u_{2,\eta,j}[i - \alpha, k])^q / \|(u_{2,\eta,j}[\cdot, k])^q\|_2$ 
     $\mu_{k,j}, \eta_{k,j} \leftarrow \arg \max_{\alpha, \eta} \rho_{k,j}[\alpha, \eta]$ 
     $a_{k,j}^q \leftarrow \rho_{k,j}[\mu_{k,j}, \eta_{k,j}] / \|(u_{2,\eta_{k,j},j}[\cdot, k])^q\|_2$ 
     $\mathcal{J}_k \leftarrow \mathcal{J}_k \cup \{j\}$ 
   $a_{k,\mathcal{J}_k}, \mu_{k,\mathcal{J}_k}, \sigma_{k,\mathcal{J}_k}, b_{k,\mathcal{J}_k} \leftarrow \text{bfgs}(R_q), a_{k,\mathcal{J}_k} \geq 0$ 
   $\mathcal{J}_k \leftarrow (\arg \text{sort}_{j \in \{1, \dots, N_{\text{ton}} + 1\}} a_{k,j} > 0)$ 
   $[1, \dots, N_{\text{ton}}]$ 
   $a_{k,\mathcal{J}_k}, \mu_{k,\mathcal{J}_k}, \sigma_{k,\mathcal{J}_k}, b_{k,\mathcal{J}_k} \leftarrow \text{bfgs}(R_q), a_{k,\mathcal{J}_k} \geq 0$ 
   $\theta_k \leftarrow \|r_k\|_2$ 
   $r_k \leftarrow (U[\cdot, k])^q - (u_2[\cdot, k])^q$ 
  if  $\|r_k\|_2 \geq \lambda \theta_k$  then
    restore values from previous iteration
  break
for  $\eta = 1, \dots, N_{\text{ins}}$  do
   $A[\eta] \leftarrow A[\eta] + \sum_{\eta_{k,j} = \eta} a_{k,j}$ 
return  $\mathcal{J}_k, a_{k,\mathcal{J}_k}, \mu_{k,\mathcal{J}_k}, \sigma_{k,\mathcal{J}_k}, b_{k,\mathcal{J}_k}, \eta_{k,\mathcal{J}_k}, A$ 

```

Figure 2. Sparse identification algorithm

partial derivative is small, taking into account the scaling of different harmonics.

Our first modification to ADAM is that while we still estimate the first moments for each dictionary entry (i.e., for each instrument and for each harmonic), we only compute one second moment estimate for each instrument, which is the arithmetic mean over the all the estimates for the harmonics.

Furthermore, we require all entries in the dictionary to be non-negative, since negative harmonic amplitudes would be unphysical. For consistency, we also require that no entries be larger than 1, so we end up with the box constraint that $D[h, \eta] \in [0, 1]$ for $h = 1, \dots, N_{\text{har}}, \eta = 1, \dots, N_{\text{ins}}$. To enforce this, we project each component to $[0, 1]$ after the end of a step.

Finally, we have to tackle the problem that dictionary entries for a particular instrument may diverge such they will not be used by the identification algorithm any more. For this purpose, we track the sum of the amplitudes associated with a specific instrument in the past. In regular intervals (every N_{prn} steps in Algorithm 1), we sort the instruments in the dictionary by their ratio of amplitude sum over the number of iterations for which they have existed (minus a small head start that benefits new instrument entries); then, we prune the dictionary by reinitializing the entries for those instruments where the ratio is lowest.

The dictionary learning algorithm and the renewal function are listed in Algorithm 3. We use the default values of $\beta_1 = 0.9$, $\beta_2 = 0.999$, $\varepsilon = 10^{-8}$, and the step-size of $\kappa = 10^{-3}$. The head start is half the length of the pruning interval: $\tau_0 = N_{\text{prn}}/2$.

function adam($D, \tau, v_1, v_2, U, k, \mathcal{J}_k,$
 $a_{k,\mathcal{J}_k}, \mu_{k,\mathcal{J}_k}, \sigma_{k,\mathcal{J}_k}, b_{k,\mathcal{J}_k}, \eta_{k,\mathcal{J}_k}$)
 $g \leftarrow \nabla_D R_{k,q}$
for $\eta = 1, \dots, N_{\text{ins}}$ **do**
 $\tau[\eta] \leftarrow \tau[\eta] + 1$
 $v_1[\cdot, \eta] \leftarrow \beta_1 \cdot v_1[\cdot, \eta] + (1 - \beta_1) \cdot g[\cdot, \eta]$
 $v_2[\eta] \leftarrow \beta_2 \cdot v_2[\eta] + (1 - \beta_2) \cdot \text{mean}(g[\cdot, \eta]^2)$
 $\hat{v}_1[\cdot, \eta] \leftarrow v_1[\cdot, \eta] / (1 - \beta_1^{\tau[\eta]})$
 $\hat{v}_2[\eta] \leftarrow v_2[\eta] / (1 - \beta_2^{\tau[\eta]})$
 $D[\cdot, \eta] \leftarrow D[\cdot, \eta] - \kappa \cdot \hat{v}_1[\cdot, \eta] / (\sqrt{\hat{v}_2[\eta]} + \varepsilon)$
 $D[\cdot, \eta] \leftarrow \max(0, \min(1, D[\cdot, \eta]))$
return D, τ, v_1, v_2
function renew(A)
 $\mathcal{I} \leftarrow (\text{arg sort}_{\eta \in \{1, \dots, N_{\text{ins}}\}} A[\eta] / (\tau[\eta] - \tau_0))$
 $[1, \dots, N_{\text{ins}}/2]$
 $\tau[\mathcal{I}^c] = 0, v_1[\cdot, \mathcal{I}^c] = 0, v_2[\mathcal{I}^c] = 0, A[\mathcal{I}^c] = 0$
for $\eta \in \mathcal{I}^c$ **do**
 $D[\cdot, \eta] \leftarrow \text{init}()$
return $\mathcal{I}, \tau, v_1, v_2, A$

Figure 3. Dictionary learning algorithm (modified ADAM)

C. Resynthesis

After the dictionary has been trained by alternating between Algorithms 2 and 3, we represent the entire recording by running Algorithm 2 on each time frame $U[\cdot, k]$ for $k = 0, \dots, n - 1$. This time, however, we need a linear-frequency spectrogram, and therefore apply the reverse transformation $f(\alpha) = f_0 e^{\alpha/\alpha_0}$ on the means of the Gaussians:

$$(z_{p,\eta}[f, k])^p := \sum_{\substack{j \in \mathcal{J}_k \\ \eta = \eta_{k,j}}} a_{k,j}^p (z_{p,\eta_{k,j}}[\alpha, k])^p,$$

$$(z_p[f, k])^p := \sum_{j \in \mathcal{J}_k} a_{k,j}^p (z_{p,\eta_{k,j}}[\alpha, k])^p,$$

with

$$(z_{p,\eta,j}[f, k])^p := \sum_{h=1}^{N_{\text{har}}} D[h, \eta]^p \cdot \exp\left(-\frac{(f - f(\mu_{k,j}) \cdot h(1 + b_{k,j}h^2)^{1/2})^2 p}{2(N_{\text{fft}}f_{\text{min}}\sigma_{k,j})^2 / (f_s\alpha_0)^2}\right).$$

For the reconstruction of the time-domain signal, we use the classical algorithm by Griffin and Lim [29] with an FFT length of N_{fft} and a sampling frequency of f_s . In order to have an identical standard deviation in the linear-frequency and log-frequency spectrograms, we choose $N_{\text{fft}}f_{\text{min}} = f_s\alpha_0$.

While more sophisticated methods have been developed recently, the algorithm by Griffin and Lim is very robust and simple. As an initial value, it accepts the original unseparated time-domain signal, namely:

$$Z[f, k] := Z(f \cdot f_s / N_{\text{fft}}, \gamma k).$$

D. Spectral Masking

As an optional post-processing step, we can mask the spectrograms from the dictionary representation with the

spectrogram from the original recording. This method was proposed in [7], [8]; we choose to modify it by taking the element-wise square root of the mask proposed therein. With, again, $p = 2$, we then have:

$$\tilde{z}_{p,\eta}[f, k] := \frac{z_{p,\eta}[f, k]}{z_p[f, k]} \cdot Z[f, k].$$

In practice, a tiny value is added to the denominator in order to avoid division by zero.

With the procedure, we make sure that the synthesized spectrograms do not have any artifacts at frequencies that are not present in the original recording. Another benefit is mentioned in [7]: In cases where the sound of an instrument is not perfectly invariant w.r.t. pitch and volume, the masking can correct this. Furthermore, the phase of the complex-valued Z provides a good approximation for the phase of the separated spectrogram.

V. EXPERIMENTAL EVALUATION

We choose a sampling frequency of $f_s = 48000$ Hz and an FFT length of $N_{\text{fft}} = 12 \cdot 1024 = 12288$. With $\zeta = 1024/f_s$, this means that we cut the windowed signal at $\pm 6\zeta$.

We aim to represent frequencies from 20 Hz up to (and not including) 20480 Hz; the log-frequency spectrogram should be $m = 1024$ pixels high. Thus, we set $f_0 = 20$ Hz and $\alpha_0 = 1024 / \ln(20480 \text{ Hz} / 20 \text{ Hz}) = 1024 / \ln(1024)$. Furthermore, we choose $\gamma = 256/f_s$. Due to $f_{\text{min}} = f_s\alpha_0/N_{\text{fft}} = 4000 / \ln(1024) > f_0$, the method from Section II-A is out of question, and we must use the method from Section II-B.

For the dictionary, we use $N_{\text{har}} = 25$ harmonics and a pruning interval of $N_{\text{prn}} = 500$ in the training.

The code is written for Python 3.5 and was tested with NumPy 1.14.3, SciPy 0.18.1, Cython 0.25.2, PyFFTW 0.10.4, Matplotlib 2.0.0, and Tensorflow 1.8.0 (for the narrowband method). It is hyperlinked in Section VII.

A. Performance Measures

Vincent et al. [30] define the signal-to-distortion ratio (SDR), the signal-to-interference ratio (SIR), the signal-to-noise ratio (SNR), and the signal-to-artifacts ratio (SAR). These measures have become the de facto standard for the performance evaluation of blind audio source separation. Assuming original signals $(X_\eta)_{\eta=1, \dots, N_{\text{ins}}}$, additive noise signals $(\Gamma_\eta)_{\eta=1, \dots, N_{\text{ins}}}$, and reconstructed signals $(x_\eta)_{\eta=1, \dots, N_{\text{ins}}}$, those quantities (to be interpreted in dB) are defined as:

$$\text{SDR}_\eta = 10 \cdot \log_{10} \frac{\|\mathcal{P}_{X_\eta}(x_\eta)\|_2^2}{\|\mathcal{P}_{X_\eta}(x_\eta) - x_\eta\|_2^2},$$

$$\text{SIR}_\eta = 10 \cdot \log_{10} \frac{\|\mathcal{P}_{X_\eta}(x_\eta)\|_2^2}{\|\mathcal{P}_{X_\eta}(x_\eta) - \mathcal{P}_X(x_\eta)\|_2^2},$$

$$\text{SNR}_\eta = 10 \cdot \log_{10} \frac{\|\mathcal{P}_X(x_\eta)\|_2^2}{\|\mathcal{P}_X(x_\eta) - \mathcal{P}_{X,\Gamma}(x_\eta)\|_2^2},$$

$$\text{SAR}_\eta = 10 \cdot \log_{10} \frac{\|\mathcal{P}_{X,\Gamma}(x_\eta)\|_2^2}{\|\mathcal{P}_{X,\Gamma}(x_\eta) - x_\eta\|_2^2},$$

where \mathcal{P}_{X_η} is the orthogonal projection on X_η , while \mathcal{P}_X is the orthogonal projection on $\text{span}\{X_\eta : \eta = 1, \dots, N_{\text{ins}}\}$, and $\mathcal{P}_{X,\Gamma}$ is the orthogonal projection on $\text{span}\{X_\eta, \Gamma_\eta : \eta = 1, \dots, N_{\text{ins}}\}$. If the noise vectors are not known (which is the typical case, unless all noise was artificially added on an otherwise completely clean signal), they are assumed to be zero, and the noise will be treated as artifacts.

The SDR is an ‘‘overall’’ performance measure that incorporates all kinds of errors in the reconstructed signal; the orthogonal projection in the numerator leads to a value of $-\infty$ if the original signal and the reconstructed signal are uncorrelated. The SIR is similar, but it ignores any artifacts that are uncorrelated with the original signals, whereas the SAR only measures the artifacts and ignores interference. The SNR (which we do not use here) measures the power of the signal compared to the power of the noise, without the artifacts. Both the SAR and the SNR are constant w.r.t. permutations of the original signals.

Originally, those measures are defined in the time-domain. This, however, makes them very sensitive to phase mismatch: The projection of a sinusoid on its 90° -shifted copy will be zero, even though the signals are otherwise identical.

We re-implemented the original MATLAB code in Python (cf. Section VII), adopting the convention to use the permutation of identified instruments with the highest summed SIR.

B. Artificial Data

To study the efficacy of the algorithm on perfectly consistent data without any artifacts or noise, we generate $N_{\text{ins}} = 2$ random instrument patterns via the init function in Algorithm 1. With this dictionary, we generate 10000 random time frames with $N_{\text{ton}} = 2$ tones at uniformly random fundamental log-frequencies $\alpha \in [0, 500)$, on which we train another dictionary. We then generate a log-frequency spectrogram with 10000 additional random time frames that we represent once with the original dictionary and once with the trained dictionary. We flatten the generated spectrogram and the spectrograms that we synthesized from the identified dictionary representations into vectors and apply the above performance measures.² The averaged result from 10 runs is displayed in Table I. No spectral masking was applied.

Table I

PERFORMANCE MEASURES FOR THE REPRESENTATION OF ARTIFICIAL DATA, ONCE WITH THE ORIGINAL DICTIONARY FROM WHICH THE DATA WAS GENERATED AND ONCE WITH A DICTIONARY THAT WAS TRAINED ON THE DATA. THE NUMBERS WERE AVERAGED OVER BOTH INSTRUMENTS AND OVER 10 RUNS WITH INDEPENDENT RANDOM DICTIONARIES AND SPECTROGRAMS. THE DENOTED UNCERTAINTY IS THE EMPIRICAL STANDARD DEVIATION.

Dictionary	SDR	SIR	SAR
Original	34.0 ± 5.7	71.4 ± 14.5	34.0 ± 5.7
Trained	32.7 ± 4.5	70.4 ± 11.3	32.7 ± 4.5

It is apparent that the algorithm is capable of achieving good separation, while the performance depends on the instrument

²Converting the spectrograms to the time-domain would not make sense, as they are almost surely inconsistent.

combinations. The difference between the representation with the original dictionary and the representation with the trained dictionary is only a fraction of the computed standard deviations, so we conclude that the dictionary learning algorithm fulfills its purpose, leaving the pursuit algorithm as the bottleneck.

C. Real Data

We used the 8th piece from the 12 Bassett Horn Duos by Wolfgang A. Mozart (KV 487) in an arrangement by Alberto Gomez Gomez for two recorders³. The upper part was played on a soprano recorder, and the lower part was played on a violin. These instruments are easily distinguishable, as the recorder has an almost sinusoidal sound, while the sound of the violin is sawtooth-like, with strong harmonics [13].

The instrument tracks were recorded separately, while a metronome/‘‘play-along’’ track was provided via headphones. Evenness of the tone was favored over musical expression. We combined the tracks by adding the two digital signals with no post-processing other than adjustment of overall timing and volume and let the algorithm run with 100000 training steps, with $N_{\text{ins}} = 2$ and $N_{\text{ton}} = 2$.

The algorithm was run with random seeds $0, \dots, 9$; the averaged results are displayed in Table II. As can be expected, the recorder is universally better represented than the violin, and spectral masking leads to considerable improvements in both domains especially for the violin. This complies with the explanation in [7] that it helps represent instruments with more diverse spectra, as the violin has 4 different strings and its sound is very sensitive to technique.

Table II

PERFORMANCE MEASURES FOR THE EVALUATION OF THE REAL DATA FOR EACH INSTRUMENT, ONCE IN THE TIME-DOMAIN AND ONCE IN THE LINEAR-FREQUENCY SPECTRAL DOMAIN. NUMBERS ARE AVERAGED OVER 10 INDEPENDENTLY TRAINED DICTIONARIES FROM DIFFERENT RANDOM SEEDS, AND HIGHER IS ALWAYS BETTER.

Masking	Domain	Instrument	SDR	SIR	SAR
Yes	Time	Recorder	14.0	28.6	14.2
		Violin	10.9	22.7	11.3
	Spectral	Recorder	13.8	34.0	13.8
		Violin	12.7	26.2	13.0
No	Time	Recorder	11.4	28.3	11.5
		Violin	6.6	23.8	6.7
	Spectral	Recorder	10.2	33.6	10.2
		Violin	8.2	29.6	8.2

For phase reconstruction, we used merely one iteration of the Griffin-Lim algorithm in order to preserve the phase of the original spectrogram as much as possible.

From subjective evaluation of the generated tracks (without looking at the performance measures), the random seed of 9 yields the best audio results. While some artifacts and interference are audible, the generated audio data provides a good aural impression of the actually played tracks. The

³[https://imslp.org/wiki/12_Horn_Duos,_K.487/496a_\(Mozart,_Wolfgang_Amadeus\)](https://imslp.org/wiki/12_Horn_Duos,_K.487/496a_(Mozart,_Wolfgang_Amadeus))

only tone⁴ that is actually misidentified is a recorder tone that interferes with the even-numbered harmonics of the violin tone that is played at the same time and is one octave lower. In this case, the third harmonic of the violin tone is erroneously identified as the recorder tone.

Spectrograms of the original recording and the synthesized representations are displayed in Figure 4. The original spectrogram contains broad-spectrum components (“noise”) that do not fit the dictionary model and thus cannot be represented, so they are not found in the synthesized spectrograms. The choice of $N_{\text{har}} = 25$ must be regarded as a compromise: Although the sound of the violin could be represented more accurately with an even higher numbers of harmonics, this would increase both the computation time of the algorithm and also the number of variables to be trained. The incorrectly identified recorder tone corresponds to the rightmost set of horizontal lines in Figure 4b. It is not audible when the synthesized audio files are mixed back together.

D. Comparison

Averaging over the first two rows of Table II, the performance figures for our algorithm are better than those achieved by [7], [8], and they are only surpassed in terms of SIR by [9]. However, the important difference is that we operate on unaltered data that was recorded from performances on actual acoustic instruments, whereas the data used in [7], [8], [9] was computer-generated from a samples database with very distinct control over the parameters. Their algorithms require tones to appear at a small set of predefined frequencies, whereas our algorithm can cope with arbitrary tones at arbitrary tuning.

VI. CONCLUSION AND FUTURE WORK

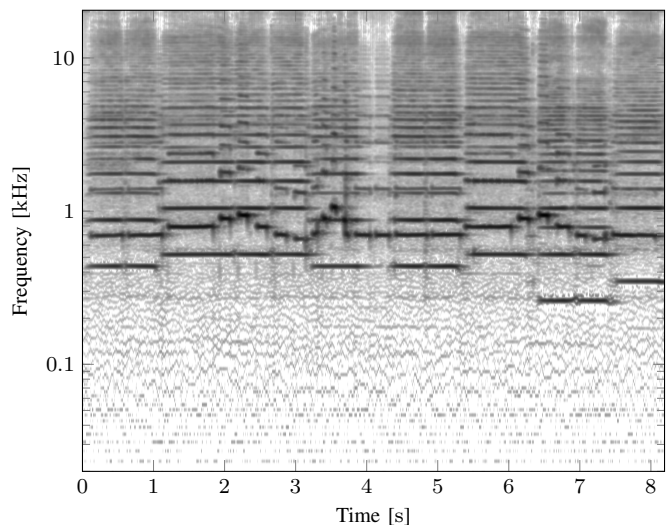
Via two novel time-frequency representations inspired by the scattering transform and by combining sparse pursuit with non-linear optimization and the ADAM algorithm that originates from the field of deep learning, we attain a blind musical instrument separation algorithm that is unique in its ability to represent and process realistic signals from actual music recordings without making any assumption about the tuning of the instruments, while maintaining performance that was previously achieved only on synthetic data.

The algorithm does not require any prior information other than the number of instruments and an upper bound for the sparsity level. It is especially suitable for instruments where the exact frequency of a tone is not fixed by the construction of the instrument but at least partly depends on playing technique.

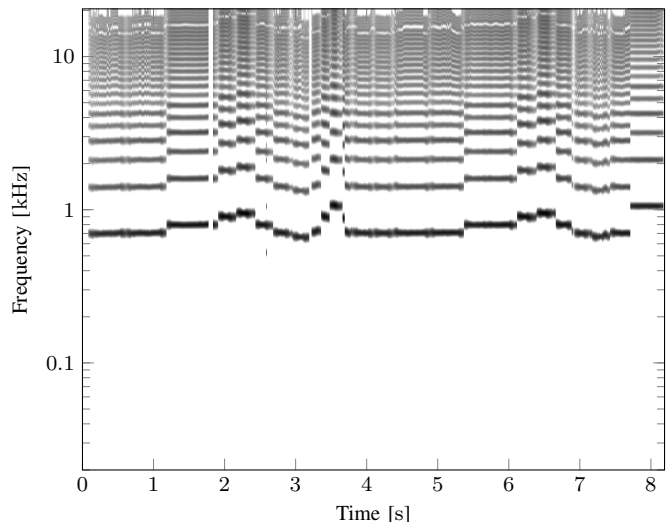
We note, however, that blind source separation always requires favorable data: Right now, our algorithm can only cope with music played on string and/or wind instruments; the spectra of the individual instruments must be clearly distinguishable by the amplitudes of the harmonics, they must be sufficiently pitch- and volume-invariant with only little overall variation in timbre, and the sparsity level must be rather strict.

The bottleneck of the presented method appears to be the pursuit algorithm, which is based on OMP. It may lead to

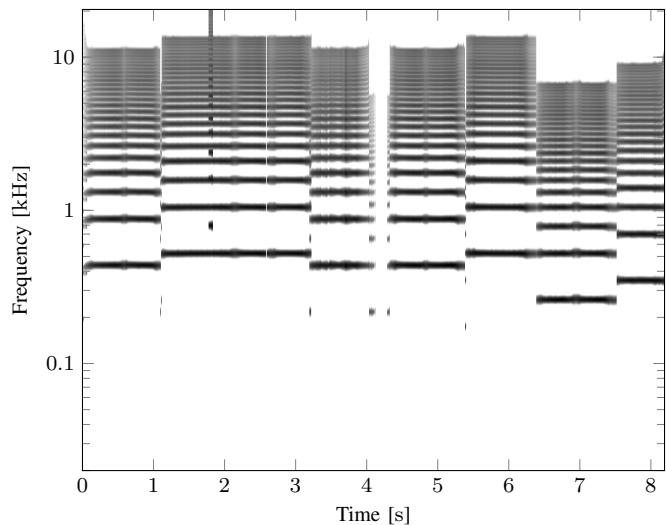
⁴which occurs 4 times in total, due to repetitions of the passage



(a) Original, generated via the wideband method



(b) Synthesized recorder track



(c) Synthesized violin track

Figure 4. Log-frequency spectrograms for the recorded piece and the synthesized tracks with a random seed of 9. The grayscale is logarithmic and normalized to a dynamic range of 100 dB for each plot.

an improvement if an ℓ_1 -based algorithm was used instead, like convolutional sparse coding [31]. The naive application of this method is hindered by the non-linear optimization step, however.

VII. RESOURCES

The software is presented along with audio samples and the original input data on the institute website⁵. The source code is available on GitHub⁶.

ACKNOWLEDGEMENTS

The first author was supported in part by DFG RTG 2224 “Pi³: Parameter Identification – Analysis, Algorithms, Implementation.”

The authors would like to thank Bernhard G. Bodmann, Gitta Kutyniok, and Monika Dörfler for engaging discussions on the subject.

REFERENCES

- [1] K. Gröchenig, *Foundations of Time-Frequency Analysis*. Springer, 2001.
- [2] D. D. Lee and H. S. Seung, “Learning the parts of objects by non-negative matrix factorization,” *Nature*, vol. 401, no. 6755, pp. 788–791, 1999.
- [3] P. Smaragdis and J. C. Brown, “Non-negative matrix factorization for polyphonic music transcription,” in *Applications of Signal Processing to Audio and Acoustics, 2003 IEEE Workshop on*. IEEE, 2003, pp. 177–180.
- [4] B. Wang and M. D. Plumbley, “Musical audio stream separation by non-negative matrix factorization,” in *Proc. UK Digital Music Research Network (DMRN) Summer Conf.*, 2005.
- [5] D. Fitzgerald, M. Cranitch, and E. Coyle, “Shifted non-negative matrix factorisation for sound source separation,” in *Statistical Signal Processing, 2005 IEEE/SP 13th Workshop on*. IEEE, 2005, pp. 1132–1137.
- [6] J. C. Brown, “Calculation of a constant Q spectral transform,” *J. Acoust. Soc. Am.*, vol. 89, no. 1, pp. 425–434, 1991.
- [7] R. Jaiswal, D. FitzGerald, D. Barry, E. Coyle, and S. Rickard, “Clustering NMF basis functions using shifted NMF for monaural sound source separation,” in *Acoustics, Speech and Signal Processing (ICASSP), 2011 IEEE International Conference on*. IEEE, 2011, pp. 245–248.
- [8] R. Jaiswal, D. Fitzgerald, E. Coyle, and S. Rickard, “Shifted NMF using an efficient constant-Q transform for monaural sound source separation,” in *22nd IET Irish Sig. and Sys. Conf.* IET, 2011.
- [9] —, “Towards shifted NMF for improved monaural separation,” in *24th IET Irish Signals and Systems Conference*. IET, 2013.
- [10] J. Andén and S. Mallat, “Deep scattering spectrum,” *IEEE Trans. Signal Process.*, vol. 62, no. 16, pp. 4114–4128, 2014.
- [11] M. N. Schmidt and R. K. Olsson, “Single-channel speech separation using sparse non-negative matrix factorization,” in *Ninth International Conference on Spoken Language Processing*, 2006.
- [12] G. B. Folland and A. Sitaram, “The uncertainty principle: A mathematical survey,” *J. Fourier Anal. Appl.*, vol. 3, no. 3, pp. 207–238, 1997.
- [13] N. H. Fletcher and T. D. Rossing, *The Physics of Musical Instruments*. Springer Science & Business Media, 2012.
- [14] W. H. Barnes, *The Contemporary American Organ*, 8th ed. J. Fischer and Bro., 1964.
- [15] P. Balazs, M. Dörfler, F. Jaillet, N. Holighaus, and G. A. Velasco, “Theory, implementation and applications of nonstationary gabor frames,” *J. Comput. Appl. Math.*, vol. 236, no. 6, pp. 1481–1496, 2011.
- [16] W. Rudin, *Functional Analysis*, 2nd ed. McGraw-Hill, 1991.
- [17] J. J. Benedetto, *Harmonic Analysis and Applications*. CRC Press, 1996.
- [18] M. Dörfler, T. Grill, R. Bammer, and A. Flexer, “Basic filters for convolutional neural networks: Training or design?” *arXiv preprint arXiv:1709.02291*, 2017.
- [19] J. A. Tropp and A. C. Gilbert, “Signal recovery from random measurements via orthogonal matching pursuit,” *IEEE Trans. Inf. Theory*, vol. 53, no. 12, pp. 4655–4666, 2007.
- [20] W. Dai and O. Milenkovic, “Subspace pursuit for compressive sensing signal reconstruction,” *IEEE Trans. Inf. Theory*, vol. 55, no. 5, pp. 2230–2249, 2009.
- [21] H. J. Nussbaumer, *Fast Fourier Transform and Convolution Algorithms*. Springer, 1981.
- [22] R. H. Byrd, P. Lu, J. Nocedal, and C. Zhu, “A limited memory algorithm for bound constrained optimization,” *SIAM J. Sci. Comput.*, vol. 16, no. 5, pp. 1190–1208, 1995.
- [23] C. Zhu, R. H. Byrd, P. Lu, and J. Nocedal, “Algorithm 778: L-BFGS-B: Fortran subroutines for large-scale bound-constrained optimization,” *ACM Trans. Math. Softw.*, vol. 23, no. 4, pp. 550–560, 1997.
- [24] J. L. Morales and J. Nocedal, “Remark on “algorithm 778: L-BFGS-B: Fortran subroutines for large-scale bound constrained optimization,”” *ACM Trans. Math. Softw.*, vol. 38, no. 1, p. 7, 2011.
- [25] D. D. Lee and H. S. Seung, “Algorithms for non-negative matrix factorization,” in *Adv. Neural Inf. Process. Syst.*, 2001, pp. 556–562.
- [26] M. Aharon, M. Elad, and A. Bruckstein, “K-SVD: An algorithm for designing overcomplete dictionaries for sparse representation,” *IEEE Trans. Signal Process.*, vol. 54, no. 11, pp. 4311–4322, 2006.
- [27] M. Aharon and M. Elad, “Sparse and redundant modeling of image content using an image-signature-dictionary,” *SIAM J. Imaging Sci.*, vol. 1, no. 3, pp. 228–247, 2008.
- [28] D. P. Kingma and J. Ba, “Adam: A method for stochastic optimization,” *arXiv preprint arXiv:1412.6980*, 2014.
- [29] D. Griffin and J. Lim, “Signal estimation from modified short-time Fourier transform,” *IEEE Trans. Acoust., Speech, Signal Process.*, vol. 32, no. 2, pp. 236–243, 1984.
- [30] E. Vincent, R. Gribonval, and C. Févotte, “Performance measurement in blind audio source separation,” *IEEE Trans. Audio, Speech, Language Process.*, vol. 14, no. 4, pp. 1462–1469, 2006.
- [31] H. Bristow, A. Eriksson, and S. Lucey, “Fast convolutional sparse coding,” in *Computer Vision and Pattern Recognition (CVPR), 2013 IEEE Conference on*. IEEE, 2013, pp. 391–398.



Sören Schulze received his B.Sc. in 2013 and his M.Sc. in 2016, both in industrial mathematics at the University of Bremen. For his master thesis, in which he began dealing with the instrument separation problem, he earned the department prize. He is currently working as a junior researcher in the Computational Data Analysis group in Bremen as a member of the DFG Research Training Group 2224. His research interests include signal and audio processing, machine learning, numerical mathematics, and applied harmonic analysis.



Emily J. King earned a B.S. in Applied Mathematics and an M.S. in Mathematics from Texas A&M University, College Station, Texas, U.S.A., in 2003 and 2005, respectively. She then received a Ph.D. in Mathematics from the University of Maryland, College Park, Maryland, U.S.A., in 2009. At Texas A&M, she was an NSF-VIGRE Fellow, Academic Achievement Scholar, and Lechner Scholar, while at the University of Maryland, she was a GAANN Fellow and Ann G. Wylie Dissertation Fellow. From 2009 to 2011, she was an IRTA Postdoctoral Fellow in the Laboratory for Integrative and Medical Biophysics at the National Institutes of Health in Bethesda, Maryland, U.S.A. She was simultaneously a Postdoctoral Research Associate with the Norbert Wiener Center at the University of Maryland. As an Alexander von Humboldt Postdoctoral Fellow, she worked from 2011 to 2013 at the University of Osnabrück, the University of Bonn, and the Technical University of Berlin, all in Germany. While in Berlin, she also was a Postdoctoral Faculty Member at the Berlin Mathematical School. Since 2013, she has been employed at the University of Bremen, Bremen, Germany, first as a Postdoctoral Researcher and now as an Assistant Professor (Juniorprofessor). She leads the research group Computational Data Analysis and does research in the fields of algebraic and applied harmonic analysis, signal and image processing, data analysis, and frame theory.

Photo credit: Uni Bremen / Kai Uwe Bohn.

⁵<http://www.math.uni-bremen.de/cda/software.html#Musisep>

⁶<https://github.com/rgcda/Musisep>